Integration of satellite-based A-DInSAR and geological modeling supporting the prevention from anthropogenic sinkholes: a case study in the urban area of Rome

Carlo Esposito, Niccolò Belcecchi, Francesca Bozzano, Alessandro Brunetti, Gian Marco Marmoni, Paolo Mazzanti, Saverio Romeo, Flavio Cammillozzi, Giancarlo Cecchini & Massimo Spizzirri

Published online: 28 Sep 2021.

Submit your article to this journal ⬀

View related articles ⬀

View Crossmark data ⬀

Taylor & Francis
Taylor & Francis Group

Integration of satellite-based A-DInSAR and geological modeling supporting the prevention from anthropogenic sinkholes: a case study in the urban area of Rome

Carlo Esposito[a] (iD), Niccolò Belcecchi[a], Francesca Bozzano[a] (iD), Alessandro Brunetti[b], Gian Marco Marmoni[a] (iD), Paolo Mazzanti[a,b] (iD), Saverio Romeo[a] (iD), Flavio Cammillozzi[c], Giancarlo Cecchini[c] and Massimo Spizzirri[c]

[a]CERI - Research Centre on Geological Risks, Sapienza University of Rome, Rome, Italy; [b]NHAZCA S.r.l., Rome, Italy; [c]ACEA s.p.a., Rome, Italy

ABSTRACT

This paper presents a methodology tuned to support the management of underground pipelines (sewer and aqueduct networks) in Rome, often threatened by the sudden formation of sinkholes related to the upward migration of existing underground cavities. The methodology integrates data coming from the assessment of susceptibility to sinkhole formation and the advanced processing of satellite-based SAR imagery. The former, performed through the multivariate logistic regression technique, relies on a detailed database of stratigraphic and other thematic (i.e. sinkhole inventory and density of underground cavities) information. A-DInSAR processing of satellite images, for which we developed on-purpose algorithms to filter only data relevant for the process under study, allowed us to provide density maps of subsiding reflectors whose likelihood to be precursors of sinkhole collapses is rated based on the integration with the susceptibility map. The procedure is addressed to point out potentially critical 'hotspots' that the company managing the underground networks should pay attention to by means of further detailed investigations. Recent (i.e. occurred after the finalization of the products shown in this paper) sinkholes validated the reliability of the procedure adopted, whose strength is the data fusion able to produce refined and focused information starting from independent and more generic datasets.

1. Introduction

Different types of geological risks threaten urban settlements, implying high levels of economic damage even in the case of hazards with relatively modest intensity due to the presence of high exposure both in terms of quantity and value. In the most

common sense, the concept of smart cities now also integrates the set of actions aimed at predicting and preventing geological hazards (Godschalk 2003; Gencer 2017). These actions will necessarily follow different approaches depending on the type of process, the administrative decision-making level (from territorial planning to regulatory plans) or management duties (for example, public or private companies that manage structures or infrastructures of public interest) and, consequently, the analysis scale (e.g. Cascini 2008).

There are several documented cases of populated areas that, in relation to the geological characteristics of the subsoil and/or anthropic actions, suffer damage due to the sudden formation of sinkholes (e.g. Kersten et al. 2017; Malinowska et al. 2019). Sinkhole is a term widely used in the recent literature to refer to surface depressions, sometimes evolving as sudden collapses, originated by a variety of underground phenomena of either natural origin, such as karstic and deep piping processes (Waltham 2008), or anthropic genesis, as in the case of excessive groundwater withdrawal (e.g. Orhan et al. 2021) or deformation/collapse of man-made underground cavities (e.g. Malinowska et al. 2019). The latter can in fact suffer instabilities that may propagate upwards and reach the surface in the form of 'anthropogenic sinkholes' with related hazard and risk implications, such as those of interest in this study. When underground cavities form dense and extended networks, as in the case of anthropogenic cavities widespread in the subsoil of Rome (Nisio et al. 2017), the problem may require large-scale zoning approaches, such as hazard analyses, already tested and applied in diverse contexts and according to a variety of approaches (e.g. Galve et al. 2009, 2011; Pradhan et al. 2014; Ciotoli et al. 2015, Parise et al. 2015; Intrieri et al. 2015; Orhan et al. 2020).

Knowledge of the spatial distribution of factors that favor the onset and development of instability processes has a key role in assessing the related spatial hazard, i.e. the identification of areas intrinsically prone to sinkhole formation. Specifically, in case of anthropic cavities – such as underground quarries – a proper spatial hazard assessment requires the knowledge of cave locations (at least in terms of zonation of their probable presence) as well as of the underground geological and hydrogeological features. In fact, lithology and water pressure and/or flow regulate the proneness of covers to undergo weathering (and related geomechanical decay), deformation and, eventually, collapse.

In the cases of collapse sinkholes, i.e. those processes evolving in sudden collapses, the prediction of time to failure could be beneficial to accomplish a complete hazard assessment, also addressed to early warning. This task, really difficult especially in presence of brittle materials in the subsoil, can be performed by measuring surface deformation anticipating the failure, as some successfully monitored cases testify (e.g. Intrieri et al. 2015; Lee et al. 2016; Nof et al. 2019; Theron and Engelbrecht 2018). Beyond the possibility to catch collapse precursors by characterizing temporal trends of deformation, monitoring is equally important in both short and middle to long term prevention to refine the spatial hazard by detecting critical areas (i.e. those with ongoing deformation). Again, with reference to sinkholes that can occur along dense and extensive cavity networks, techniques such as satellite SAR interferometry (e.g. Chang and Hanssen 2014; Abspoel et al. 2018; Malinowska et al. 2019) have the

advantage of providing a high spatial density of information on wide areas, especially in an urban environment rich in signal reflectors. This ensures adequate geometric and temporal resolution in medium to large scale analyses. Useful management and prevention methods in defense of linear infrastructures and pipelines are represented by solutions based on data assimilation (Vaccari et al. 2018; Abspoel et al. 2018). Such an approach can be adopted for the specific problem of anthropogenic sinkholes by integrating the advantages of a susceptibility analysis of the territory, capable of identifying potentially critical areas based on quasi-static factors (i.e. cavity density and geological setting of the subsoil), with a monitoring capable of highlighting areas where an instability process is actually in progress. This work summarizes the results of a research carried out in collaboration with ACEA s.p.a., the company that manages the aqueduct and sewage infrastructures of the city of Rome, where in some specific sectors sudden collapses of pre-existing underground caves cause damage to the infrastructures themselves and consequent interruptions of service. Given the peculiar spatial pattern of both the instability and the pipeline networks, linearly distributed over a large territory, an integrated methodology has been developed on the basis of the data assimilation criterion capable of making the information drawn from satellite SAR interferometric (A-DInSAR) monitoring more effective by coupling it with a susceptibility zoning based on geological predisposing factors. In fact, A-DInSAR monitoring provides important information, even at high resolution, on deformations in progress, but this information cannot be used to infer the causes unless supported by a meta-information that captures the intrinsic characteristics of the subsoil and, therefore, of the possible causes of the observed effect, at least in terms of likelihood. Therefore, the methodology relied on two cornerstones independently developed and subsequently integrated:

1. 3D geological model of the study area has been reconstructed and a spatial hazard analysis of the territory has been performed based on geological conditions predisposing to collapse sinkholes.
2. A-DInSAR elaborations of SAR satellite data and related post-processing algorithms have been tuned, aimed at filtering only the data that are reasonably referable to potential precursors of collapse of underground cavities, according with location, radiometric and displacement characteristics. In view of possible applications for temporal prediction of collapse, some selected cases of recently formed sinkholes have been back-analyzed to assess the potential of SAR interferometry in the site-specific context to catch and typify precursor trends of displacement.
3. The two products have been overlaid to provide a more reliable 'real time' territory zoning in terms of sinkhole spatial hazard, accounting for both 'static' proneness (i.e. presence of cavities and geological setting) and 'dynamic' information of ongoing instabilities (i.e. clusters of subsiding scatterers)

The developed method represents the rationale for the operational-management tool that ACEA is testing for effective prevention of damages of buried linear infrastructure due to sinkhole formation.

2. Geological setting

The city of Rome lies in a hilly area surrounding the Tiber river valley (Figure 1a). From a geological point of view, its configuration is the result of repeated depositional events of sedimentary and volcanic genesis that followed one another, alternating with erosive phases, during the Plio-Pleistocene period (Marra and Rosa 1995; Marra and Florindo 2014). The common geological bedrock of the city is featured by a thick sequence of Pliocene marine clays (Monte Vaticano Formation). Lower Pleistocene coarser sediments (silty sands of the Monte Mario Formation) testify for a gradual continentalization of the environment, which resulted in the deposition of littoral, transitional and continental sediments (Ponte Galeria Formation) during lower-middle Pleistocene. These deposits largely outcrop in the hills on the right bank of the Tiber. A subsequent succession of alternating volcanic deposits (originated by several volcanic districts located north and south of the city that activated about 600 ka ago) and continental (mainly alluvial and palustrine) sediments deposited in the area during middle-upper Pleistocene. A significant thick sequence of volcanic deposits fed by the Colli Albani Volcanic District (CAVD), located south of Rome, characterizes the subsoil of a large part of the city on the left bank of the Tiber river (Figure 1b).

Among the volcanic units of the CAVD, 'Pozzolane Rosse' *Auctt.*, 'Pozzolane Nere' *Auctt.* and 'Tufo Lionato' *Auctt.* (listed from the elder to the younger and labeled as RED, PNR and VSN_1, respectively, in the CARG official geological map; Figure 1b) have to be mentioned, as the related deposits have been largely exploited – often in underground quarries – as construction materials since the ancient Roman age and play a relevant role in this study. These units are featured by massive pyroclastic deposits related to ignimbritic flows; from a technical point of view, RED and PNR are very weak rocks, while VSN_1 in terms of compressive strength lies at the border between weak rocks and proper lithoid rocks.

Recent alluvial deposits of the Tiber river and related tributaries, with thicknesses up to tens of meters, locally overlie the Pleistocene sequence; finally, it is worth mentioning the presence of backfill with even significant thickness, 'stratified' during the long history of the city.

2.1. Overview on the anthropogenic sinkholes in the city of Rome

Among other natural and anthropogenic hazards, the city of Rome suffers the damages due to widespread – and often sudden – formation of ground collapses (Figure 2), framed in different geological-geomorphological and anthropic contexts.

ISPRA (the Italian Institute for Environmental Protection and Research, which hosts the Italian Geological Survey) manages a project (http://www.isprambiente.gov.it/it/progetti/suolo-e-territorio-1/il-progetto-sinkhole/sprofondamenti-nelle-aree-urbane) to study these anthropogenic sinkholes, that are considered as a proper risk factor for the city. In the frame of this project, ISPRA inventoried a huge number of sinkholes occurred in the last 150 years and provided a first, large-scale assessment of the territory proneness to collapses in the urban area (Ciotoli et al. 2015). Most of the inventoried sinkholes are clustered in a specific sector of the city (Figure 3a), featured by the presence of volcanic deposits (i.e. 'Pozzolana') with excellent characteristics for building purposes and thus
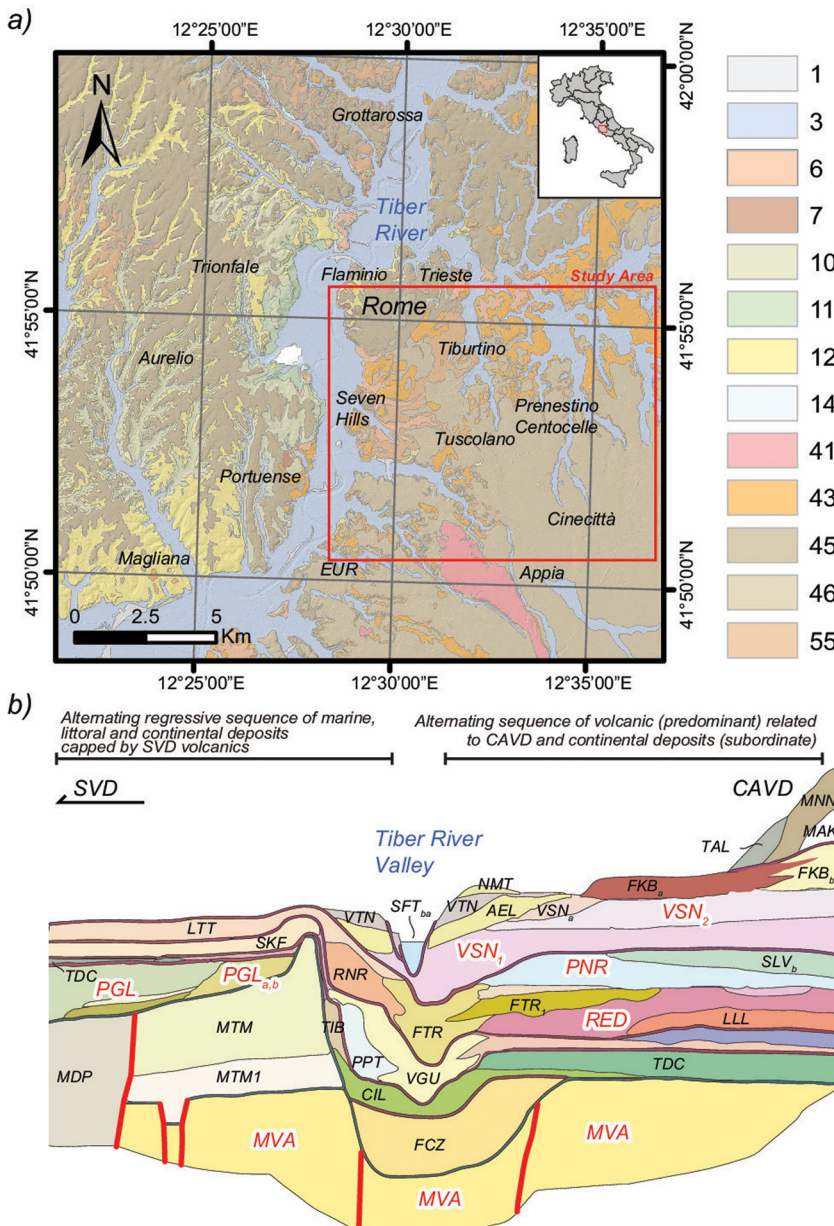
Figure 1. a) Litho-technical sketch map of the Rome urban area. The extent of the study area is outlined by the red rectangle; b) Stratigraphic scheme of the Roman area across the Tiber River Valley; labels refer to the code of geological units and formations adopted in the official geological map (CARG), modified after Funiciello and Giordano (2008). Key to legend: 1) Anthropic deposits; 3) Recent and terraced sandy-gravelly alluvial deposits, eluvio-colluvial deposits; 6) silty-sandy alluvial deposits, fluvio-lacustrine deposits; 7) travertines; 10) Plio-pleistocene clayey and silty deposits; 11) Marine Pliocene clays; 12) Debris and talus slope deposits, Conglomerates and cemented breccias; 14) Marls, Marly limestones and calcarenites; 41) Leucititic/trachytic lavas; 43) Lithoid Tuffs, Pomiceous ignimbritic and phreatomagmatic facies; 45) Welded tuffs, tufites; 46) Pozzolanic sequence; 55) Alternance of loose and welded ignimbrites; labels in red highlight the units/formations mentioned in this paper.

Figure 2. Example of a sinkhole occurred in 2017 within the study area. a) General view of the sinkhole (photo credits: https://roma.repubblica.it) and b) detail showing the presence of anthropic structures, thus testifying for the preexistence of anthropogenic underground cavities (photo credits: Francesco Fotia / AGF).

exploited as a mineral resource since the ancient Rome age. Therefore, a large part of the city is characterized by the presence of a very dense network of underground cavities (Figure 3b); only few of them have been recognized and carefully mapped, also due to the difficulty in exploring these tunnels, frequently interrupted by roof collapses. Furthermore, other underground cavities are related to ancient hypogeal construction, such as catacombs.

The durability of such tunnels is strictly related to the mechanical properties (and related decay due to weathering over time) of deposits at the tunnel crown, as well as to the entity and quality of the overlying cover: the former controls the lithostatic load (and the formation of the soil-arch effect), while the latter governs the long-term stability, water infiltration and related weathering. Bianchi Fasani et al. (2011) provided an observation-based evolutionary model to explain the upward migration of tunnel crown of preexisting tunnels in the volcanic subsoil of Rome up to the formation of sinkholes (Figure 4), that can develop as a stepwise sequence of steady-state and low-rate deformations (weathering) interspersed with sudden increases in
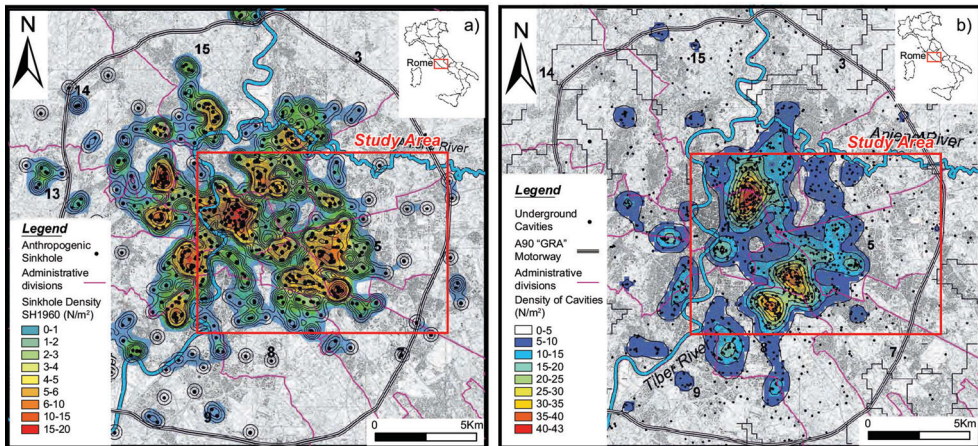
Figure 3. Density maps of sinkholes (a) and underground cavities (b) in the urban center of Rome according to Ciotoli et alii 2015. Basemap modified after Ciotoli et al. 2015.

deformation rate (partial roof failures) up to the possible formation of a ground collapse. It is worth noting that due to the mainly brittle behavior of cap rocks (especially tuffs) such collapses can occur as sudden failures preceded by low deformations, thus affecting the possibility of an effective monitoring for early-warning purposes. Even if no significant damages to buildings have been ever recorded, this kind of process frequently involves roadways causing damages to vehicles and buried service infrastructures (e.g. water supply and gas pipelines, sewer systems, power lines). Water leakages from pipelines and the 'draining trench effect' of linear excavations performed for subway service infrastructures and backfilled with permeable materials, are sometimes claimed as predisposing factors. It is worth noting that several collapses occurred and still occur in natural areas, never urbanized in recent times and, thus, neither crossed by modern pipelines. This evidence claims a relevant role of subsoil geology as a predisposing factor, at present not properly focused on the land management scale.

3. Materials and methods

Since the anthropogenic sinkholes above described affect a specific portion of the urban area the comprehensive, integrated methodology has been tuned and refined in a study area featured by the concomitant presence of favorable geological setting, underground cavity networks and sinkholes, as well as covered by a dense and homogeneously distributed dataset of boreholes allowing to support the subsoil reconstruction (Figure 5).

The methodology is focused on data assimilation: the 'susceptibility assessment' – spatial hazard zoning based on 'static' information (Figure 6a) – drives the interpretation of actual ground displacements ('dynamic' information) detected by means of satellite A-DInSAR. Specifically, for this study, the multi-temporal interferometric analyses have been carried out by using the Persistent Scatterers Interferometry (PS-InSAR or PSI) technique (Ferretti et al. 2000; Ferretti et al. 2001; Hanssen 2005; Kampes 2006). PSI technique, in fact, proved to be effective for the detection of displacements affecting urban areas, structures and infrastructures (Gernhardt et al.
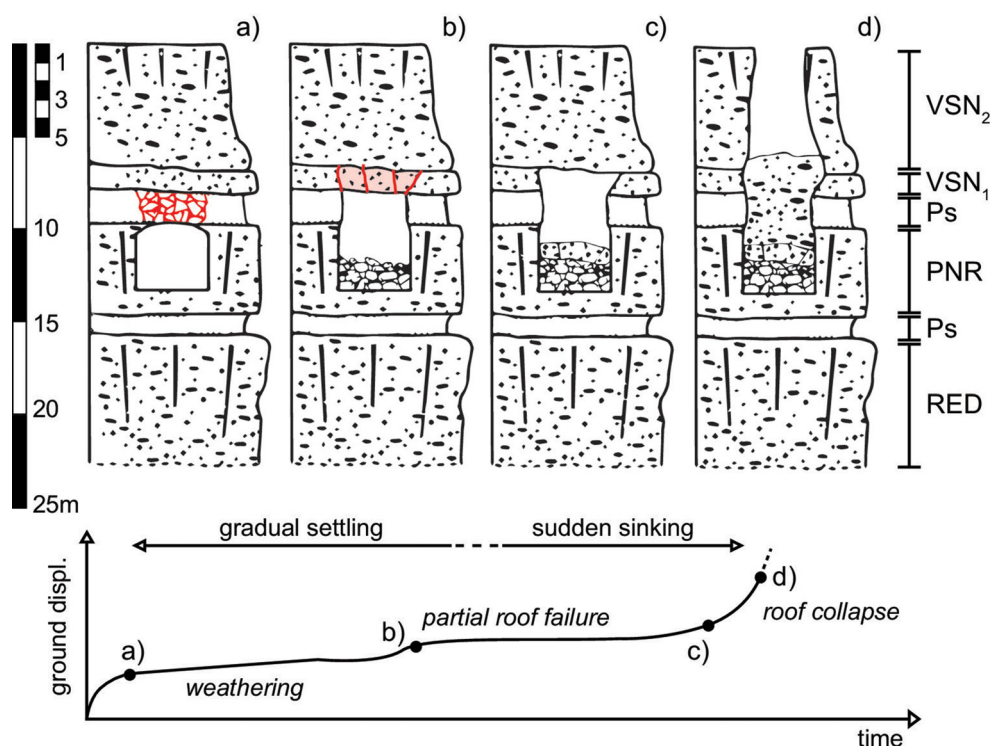
Figure 4. Evolutionary model of upward migration of instability/weathering at the roof of pre-existing tunnels in the volcanic subsoil of Rome up to the formation of sinkholes. Upward migration of tunnel crown from original cavity in the Pozzolane Nere Auctt. (PNR sensu CARG, Funiciello and Giordano 2008) by subsequent collapses or spalling involving the Tufo Lionato (VSN$_1$) and Pozzolanelle (VSN$_2$) and interlaying paleosol (Ps). Modified after Bianchi Fasani et al. (2011). The graph in the lower part qualitatively shows the alternation of steady-state and low-rate deformations (weathering) interspersed with sudden increases in deformation rate (partial roof failures) up to the possible formation of a ground collapse.

2010; Bozzano et al. 2018; Wang et al. 2018; Bozzano et al. 2020). Moreover, post-processing approaches have been specifically calibrated to adapt the analysis to the site-specific context and process. The final result is the definition of maps of deforming Persistent Scatterers (PSs) (Figure 6b).

Afterwards, the obtained results were integrated basically through the attribution of a sinkhole susceptibility level to each identified deforming zone (made up of clusters of deforming points), thus ranking their likelihood to be actually representative of a precursor of a ground collapse (Figure 6c). This integrated information is crucial to support and address stakeholders, such as companies managing service infrastructures, in defining priorities for prevention/protection actions (e.g. detailed investigations and/or monitoring and/or interventions).

3.1. Sinkhole susceptibility assessment

The final aim of the susceptibility assessment is the zonation of a portion of the municipal territory, resulting from the analysis of the time-invariant geological factors
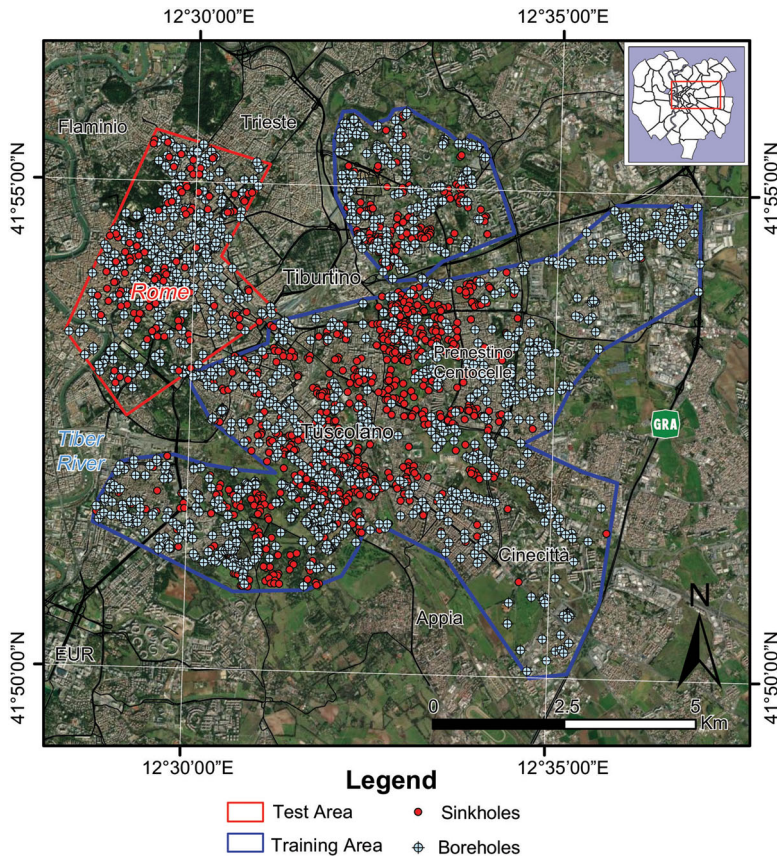
Figure 5. Detail of the study area. The blue and red polygons outline the training and test areas of the susceptibility analysis, respectively. Distribution of the available boreholes supporting the subsoil reconstruction and the location of inventories sinkholes are also shown.

that condition/predispose the formation of the specific type of anthropogenic sinkholes above described. The basic assumptions for the selection of the geological variables rely on the evolutionary model studied and conceptualized in the work by Bianchi Fasani et al. (2011).

To provide informative layers representing the selected variables, the susceptibility assessment requires preparatory actions, such as the construction of the geological model and the inventory of occurred sinkholes, to measure – in qualitative or quantitative terms – the strength of the cause-and-effect relationship.

Compatibly with the data availability, in terms of quantity, quality, spatial density and homogeneity of the information, a high-resolution geological model of the subsoil volume in which the cavity network is hosted is a key tool to better understand and frame the role of relevant information, i.e. those related to:

- the presence and the thickness of 'Tufo Lionato' (VSN_1), having fairly good mechanical properties, that stratigraphically overlies the 'Pozzolane Rosse' (RED) and 'Pozzolane Nere' (PNR) and the tunnels dug therein, thus acting as a supporting beam;
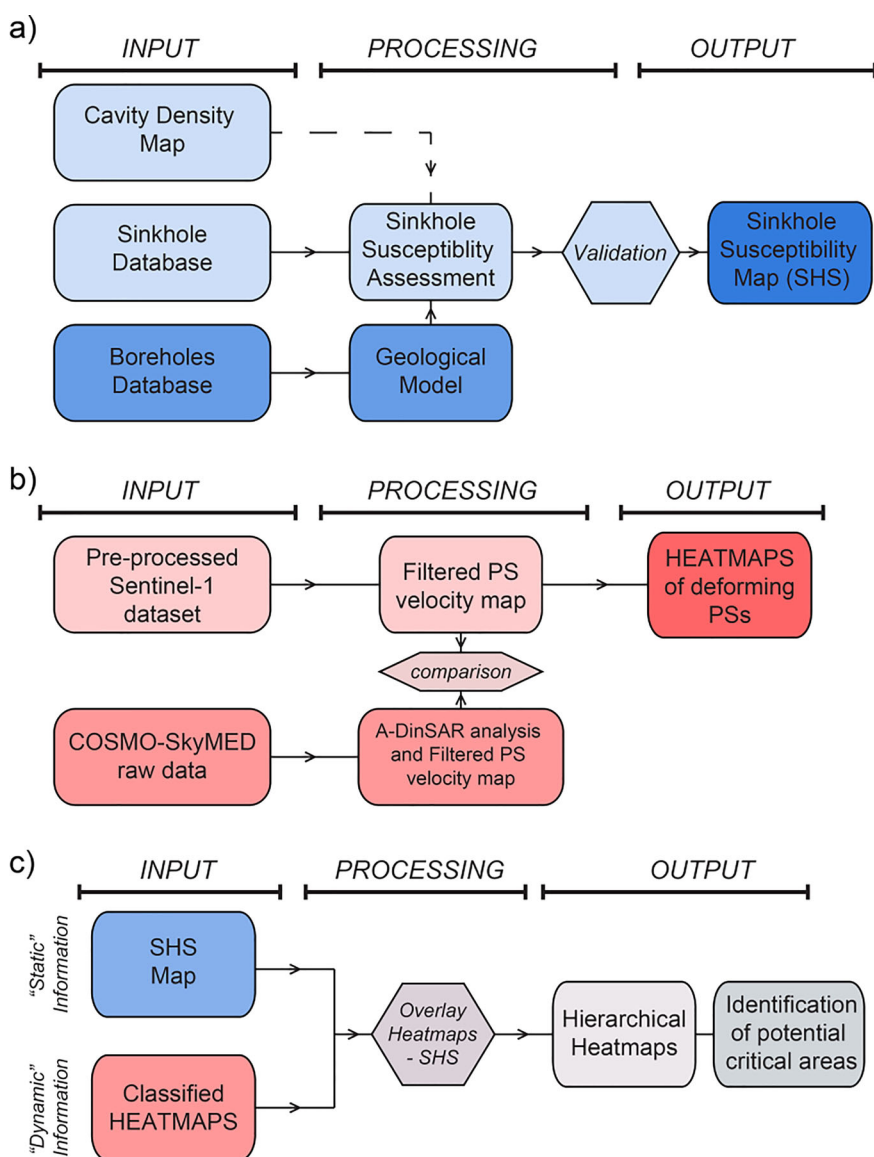
Figure 6. Workflows illustrating the main steps of: susceptibility assessment and related mapping (a), SAR processing for identification and mapping of subsiding PS clusters (b), data integration and related spatial hazard zoning (c).

- the depth below the ground level of the upper limit of RED and PNR (if present), considered as a proxy of cavity network depth, which has implications in the long-term stability of tunnels and on the effective possibility for roof collapses/ degradation to reach the ground surface.

With the aim of assessing the spatial variability of target geological information, starting from the collection of available data (Ventriglia 2001) a georeferenced database of stratigraphic logs has been designed. As a first step, a challenging activity of

re-interpretation of stratigraphic information, usually available as raw descriptions, has been performed to filter and homogenize data. Each identified layer has been attributed to one of the formal units of the official geological map. Operating in an open-source GIS environment, from this database we extracted information on the depth b.g.l. and altitude a.s.l. of top and bottom of the layers featuring the stratigraphic succession of each stored borehole. Then we interpolated the so-obtained data to achieve continuous information by applying the Inverse Distance Weighting technique; the interpolation was confined in polygons where the data density has been considered satisfactory (Figure 5). Additional information such as the thickness and related spatial variability of the layers have been produced by means of GIS-based processing.

The collection, digitization and vectorization of available data about the location of sinkholes (Ciotoli et al. 2013; Ciotoli et al. 2015) has been integrated with additional web-based research (mainly archives of local newspapers); then we set up a database containing 1016 sinkholes that occurred in the period 1875–2018 (Figure 5).

Based on GIS elaborations (i.e. overlay of sinkhole locations on geo-thematic rasters and sampling of the related values), we created a vector layer made up of points corresponding to sinkhole location and related attributes containing information on the elevation a.s.l. and depth b.g.l. of top and bottom of each underlying geological formation.

To analyze the relationship between causative factors and sinkhole occurrence, a susceptibility assessment by means of the logistic regression (LR) multivariate statistical technique has been performed. Logistic regression is a widely used technique to explore statistical relation between 'independent' variables (i.e. representing the preparatory factors) and the 'dependent' variable (i.e. sinkhole occurrence), properly described as a dichotomous variable: '0' for absence and '1' for presence. Furthermore, by applying the Logit function it is possible to express the probability of each single terrain unit (5-meter square grid cell in this case study) to assume the value '1', i.e. to undergo a sinkhole collapse.

Starting from the geological information associated with each sinkhole, the analytical approach consisted of a GIS-based stepwise procedure.

A first exploratory phase consisted in the identification of the most relevant geological variables by evaluating the frequency distribution of sinkholes vs. depth and thickness of each geological layer, in turn, derived from the 3 D geological model. The choice of controlling geological variables has been based on the evolutionary model by Bianchi Fasani et al. (2011) according to which: (i) shallow cavities are directly influenced by external loads (e.g. traffic and/or man-made structures) and easily subject to weathering by seepage, (ii) the higher is the thickness of deposits with beam function in the calotte, the lower is the proneness to roof collapses;

Afterwards, we prepared an additional informative layer representing the density of known cavities, as their presence is a necessary condition for the occurrence of the specific type of sinkhole under investigation. In other terms, this additional information represents a proxy of the probability of the presence of underground cavities, useful to grade the likelihood of sinkhole occurrence, the geological setting being equal. Starting from an available inventory (Nisio et al. 2017), on purpose

georeferenced and digitized, we populated a Geodatabase and then produced a cavity density map using a Kernel Density function. With a procedure similar to the above described, a density map of sinkhole events has been produced.

Finally, we extracted the datasets representing the combination of variables leading to sinkhole formation (i.e. dependent variable equal to 1) and those associated with sinkhole absence (i.e. dependent variable equal to 0). The datasets that represent the dependent variable have been prepared as follows. As regards the population '1', all the inventoried sinkholes have been collected and stored in a Geodatabase. With reference to the value '0', we created a random dataset of points in the study area and we then selected only points enough far from known collapses, thus ensuring a reliable evaluation of 'stability' in that given point. For this purpose, the density map of sinkhole events has been used to avoid sampling stable points in areas close to inventoried sinkholes.

For further validation, this dataset has been split into two subsets: one related to a larger area and another to a smaller one (Figure 5). The former was used to explore the relationships between geological setting and sinkhole occurrence and, thus, train the susceptibility function; the latter has been excluded from the exploratory phase and used to test the predictive capability of the susceptibility function. The latter has been constructed by applying the LR technique to the training dataset in the following form:

$$Y = Logit(p) = \ln(p/1 - p) = \hat{\alpha} + \hat{\beta}_1 x_1 + \hat{\beta}_2 x_2 .... \hat{\beta}_n x_n$$

The results have been expressed in terms of the probability of each cell to assume value '1' by applying the following formula:

$$P[(Y = 1|x_i)] = \frac{1}{1 + e^Y}$$

The validation consisted in verifying the correspondence between predicted susceptibility values and the location of the actual sinkholes in the test area, not used for training; to quantitatively express the predictive capability of the model ROC curves and related AUC values have been calculated. Once validated, the susceptibility function (in terms of spatial probability) has been applied to the whole study area: the resulting map has been also reclassified into a finite number of sinkhole susceptibility (SHS) classes.

3.2. Interferometric analysis

Selecting the most reliable PS can improve the efficiency of A-DInSAR techniques, such as the PSI used in this study, for the detection of some specific hazard processes, especially in urban areas. In fact, on one hand, the urban environment offers a huge number of good scatterers, on the other hand, data can often be very 'noisy' due to other effects (e.g. soil deformation induced by excavations/constructions, structural building instabilities and/or thermal deformation, etc.). Therefore, the method developed in this study consisted in tuning a series of algorithms to implement an automated stepwise procedure based on multiple criteria for filtering the huge number of PS (and related time-histories of displacement) usually available in urban contexts and selecting those more likely related to sinkholes.
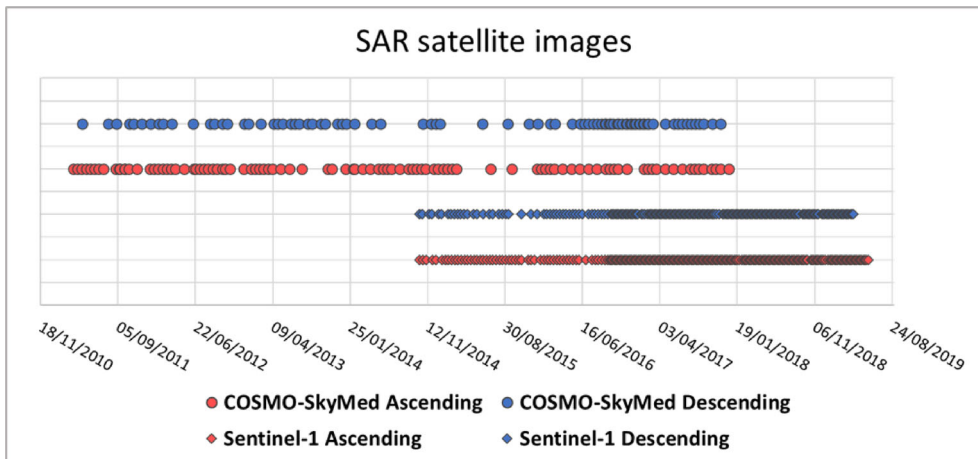
Figure 7. Temporal distribution of the SAR satellite datasets used in this study.

The reliability of the procedure and the time-space resolution of the PSI analyses in locating and registering deformations anticipating the paroxysmal phase of a sink-hole occurrence were tested. Both Sentinel-1 (European Space Agency) and COSMO-SkyMed (Italian Space Agency) datasets have been hence handled, processed and compared to get some hints about the cost-benefit of the related products.

3.2.1. Validation and post-processing of A-DInSAR data from sentinel-1

The analyses were based on interferometric products supplied by ACEA, derived from the processing of Sentinel-1 images of the European Space Agency performed and provided by third parties. Such products consisted in velocity maps of the PSs in double orbital geometry (ascending and descending) which include the following key information:

i.   geolocation of individual PSs;
ii.   average annual velocity values of PSs;
iii. PS phase temporal coherence values;
iv.   time series of cumulative displacement of the PS obtained from the individual measurements;
v.   other auxiliary data (including the PS elevation);
vi.   PS backscattering amplitude.

These data, which cover a time interval between October 2014 and May 2019, were obtained from the analysis of 214 images in ascending orbital geometry and 192 images in descending orbital geometry, with 6- and 12-days revisit time and spatial resolution of 5×20 m. It is worth noting the datasets provided by ACEA are the result of A-DInSAR analyses performed using only linear models. In Figure 7, the temporal distribution of the Sentinel-1 SAR images is reported for both the orbital geometries. It is worth noting that since the processing of data was performed by third parties, no baseline plots could be retrieved.

Based on this dataset, the procedure follows the workflow below described in which every step has been implemented by means of specific algorithms developed on purpose:

(1) Discrmination of PSs based on their location (on the ground or on buildings) and selection of those reliable for the analysis, i.e. on the ground. This criterion was adopted starting from the following assumptions:
   - most of the inventoried sinkholes occurred on roadways;
   - the aqueduct and sewerage networks are mainly below the roadways;
   - PSs located on buildings could potentially be affected by effects related to the static behavior of the structure, even independently of the interaction with the foundation soil.
(2) PS filtering based on phase coherence. This parameter represents the level of correlation between the measured data and the deformation model adopted in the interferometric analyses. The coherence values vary from 0 (totally devoid of correlation with the model) to 1 (data perfectly correlated with the model). PSs with coherence values under a selected threshold have been excluded in order to filter only the most reliable targets.
(3) PS filtering based on the standard deviation of the time series of displacement. This step represents a refinement of the filtering based on the phase coherence. As known, although PSI provides high values of accuracy (in the order of some mm) in the measurement of PS velocity (trend) over long data acquisition periods, single measures can show significant fluctuations, due in part to residual atmospheric disturbances and partly to the background noise of the reflector. However, it is possible to consider this dispersion as an index of the quality of the PS and, therefore, through appropriate thresholds on the standard deviation values, filtering only the most reliable PSs. The time series of displacement of all available PSs were analyzed in order to calculate the standard deviation and select only PSs with standard deviations within a specified range.
(4) PS filtering based on velocity threshold and the sense of displacement. The accuracy of A-DInSAR techniques in the measurement of average annual velocity is very high. However, unlike other monitoring techniques, it is not possible to define a priori standard values of instrumental accuracy, as this parameter depends significantly on several factors such as, for example, those related to residual atmospheric artifacts, the intrinsic characteristics of the reflector itself and the background noise. For this reason, a detailed site-specific analysis is appropriate for the identification of a reasonable value of accuracy, statistically valid for the dataset (and, therefore, for most of the PSs contained in it) and thus to discriminate points that record displacements from points that, on the contrary, do not detect anomalies or, in any case, anomalies in a non-representative range. Furthermore, only PSs with a sense of movement away from the sensor (i.e. the direction of movement expected for surface sinking phenomena) are selected.
(5) In addition, the procedure implemented a parallel algorithm for the identification of temporary scatterers, which with high probability would be eliminated

with the only coherence filtering, this being calculated over the entire analyzed period and not only on the time interval in which the temporary scatterer is actually present. The algorithm uses both the displacement dataset and the amplitude dataset, allowing the values that are related to outliers in the amplitude values (referring to anomalous signal reflections, with respect to the historical series) to be removed from the individual time series of displacement. Then it identifies the 'T$_{on}$' and the 'T$_{off}$' (temporal instants of appearance and disappearance of the temporary scatterers, respectively) and recalculates the displacement trends for the only period in which the single scatterer is present (and, consequently, the average PS velocity). By convention, for a PS to appear/disappear to be considered suitable for post-processing, the time period in which the scatterer is 'on' must be at least one continuous year.

(6) Production of maps representing the concentration of (filtered) subsiding PSs: the high density and redundancy of information achievable by PSI, is suitable to facilitate the interpolation of information in a given neighborhood, allowing the identification of 'clusters' where there is a high concentration of data that meet certain predefined criteria. In particular, it is possible to identify areas characterized by the presence of PS with anomalous but redundant behavior and therefore to obtain products (concentration maps) that are configured as a valid tool to support the interpretation of the interferometric data and the spatial predictability of the triggering of instability phenomena. Starting from the filtered and selected PSs, an algorithm based on the Kernel Density Estimation (KDE) function was adopted for the identification of clusters of points with deformational trends over the above thresholds and generation of related heatmaps (i.e. concentration maps colored on the basis of filtered PS density). When using the algorithm, the following parameters must be specified:

(a) the radius (h), which influences the spatial neighborhood to consider for the assignment of values at each point;

(b) the Kernel function, that controls the decreasing influence of the point (PS) with the increase of the distance from it. This function allows the calculation of the density value at a point 'z' (estimation point) knowing the distance 'd' from a reference point (PS). In this case, the density value also considers the velocity of the measurement points (VelPS). The distance ì'd' is calculated in terms of Euclidean distance, then normalized with respect to the chosen radius. Finally, it is necessary to consider the cases in which a point is in the area of influence of several PSs. In this case, the assigned value results from the sum of all density values obtained from each PS in the range.

3.2.2. Validation and comparison with COSMO-SkyMed data

The reliability of the analyses carried out with Sentinel-1 datasets was tested by back-analyzing recent collapse events with a known date of occurrence, to validate the capability of processed SAR products to catch deformations anticipating the paroxysmal phase. To further assess the performance of Sentinel-1 imagery by a comparative
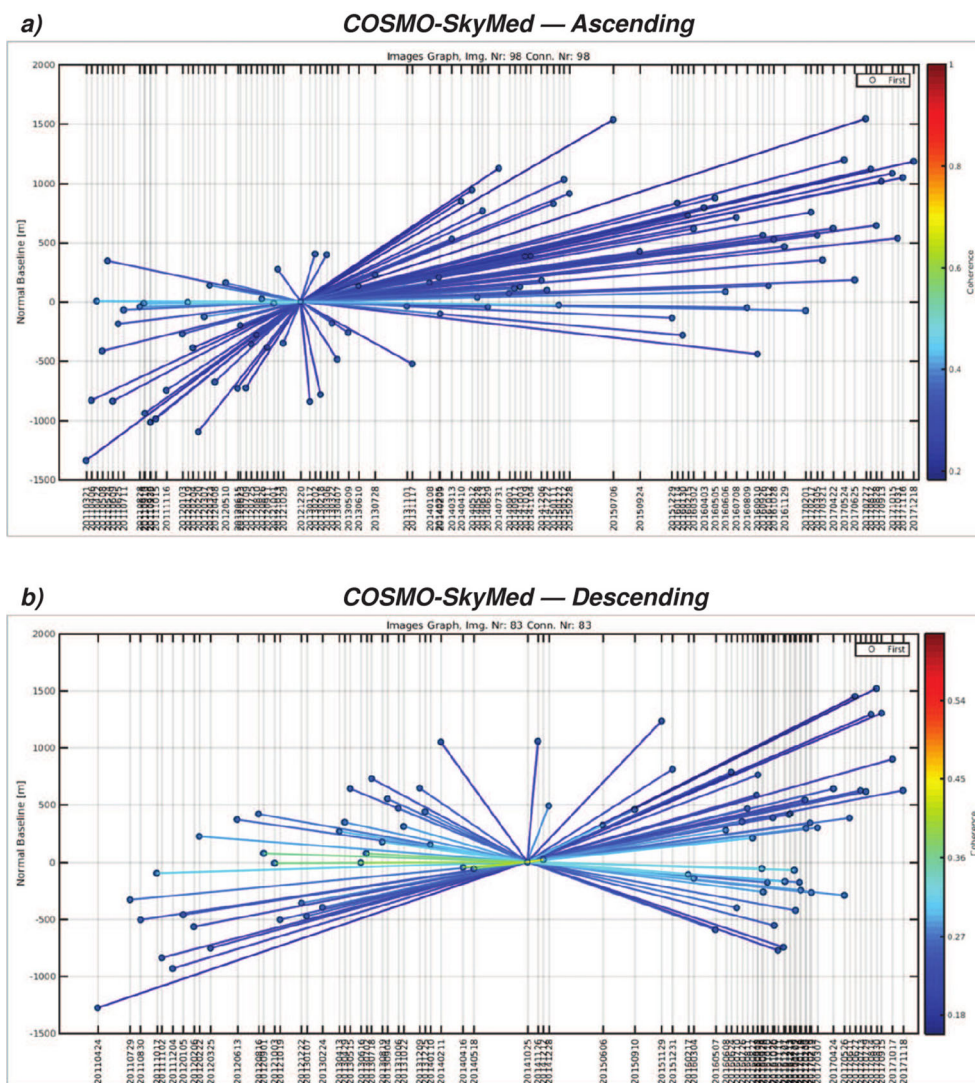
Figure 8. a) Normal baseline vs Temporal baseline plot with the Star graph for the PSI analysis of the COSMO-SkyMed ascending dataset. b) Normal baseline vs Temporal baseline plot with the Star graph for the PSI analysis of the COSMO-SkyMed descending dataset.

evaluation, the same analysis was performed with the same procedure on COSMO-SkyMed (CSK) SAR data characterized by a lower temporal resolution (revisit time ranging between 16 and 32 days) but a higher spatial resolution (3×3 m). In particular, we processed a CSK data stack (already available in the CERI archives) consisting of 98 SAR images in ascending orbital geometry and 83 SAR images in descending orbital geometry that cover a time interval between the first half of 2011 and the end of 2017 (i.e. wider than the Sentinel-1 stack) (Figure 7).

The CSK data were processed entirely by means of the PSI technique (Figure 8) starting from the raw information up to the filtered dataset and related heatmaps. This allowed us to implement an additional and more refined analysis, using linear

deformation models (for the purpose of an objective comparison with the Sentinel-1 products) and non-linear models, aimed at identifying any PS characterized by a non-constant rate of deformation over time, whose velocity or cumulative displacement values can be underestimated, or even excluded, from the analysis with a linear model.

3.2.3. Data integration

The overlay and intersection in GIS environment of the outcome of PSI analyses and related heatmaps ('dynamic' information) with the susceptibility map ('static' information) allowed us to produce a synthetic information able to assign an indication of likelihood of each hotspot of deforming PS clusters to be a precursor of cavity collapse, based on the local (and independent) estimation of susceptibility. In other terms, this stage basically consisted of a subclassification of the heatmaps based on a sinkhole susceptibility criterion.

4. Results

4.1. Susceptibility assessment

The GIS-based intersection of sinkhole location and geo-thematic information allowed us to explore the relation between ground collapses and geological setting, the latter being declined by some selected parameters, such as thickness, depth to top and bottom of different units and other synthetic information (e.g. ratio of thickness to the depth of top/bottom of different layers) resulting from a 3 D geological model obtained through the interpolation of geological data associated with the boreholes stored in the database.

A preliminary, simple descriptive statistic such as frequency distribution of each classified variable allowed us to highlight the role of some geological parameters which are consistent with the evolutionary model by Bianchi Fasani et al. (2011). After different attempts of variable classifications in terms of class width, the strongest – or at least the most interpretable – relations are given by:

- the presence and thickness of VSN_1 which acts as an efficient 'roof' of the cavities since it is the best possible layer from a mechanical point of view;
- the depth at which the top of VSN_1 is located with respect to the surface, which in some way measures the extent of the loads acting on the supporting beam of the cavities;
- the proportion of VSN_1 to the total thickness of deposits above the top of PNR or RED, that are proxies of the potential underground cavity level, which provides indications on the 'quality' of cover deposits.
  Specifically:

- The thickness of VSN_1 divided into equal classes of 2 meters shows a frequency distribution consistent with the assumption of its enhanced capacity to bear loads and stress distribution due to the tunnel arch effect: the smaller the thickness, the greater the sinkhole frequency (Figure 9a).
- the frequency distribution of the depth at which the top of VSN_1 is located with respect to the surface, divided into 5 meters wide classes, reflects the enhanced protection of cavities from weathering effects due to water seepage as well as from the transfer of external load (e.g. road traffic and any other man-induced stress from
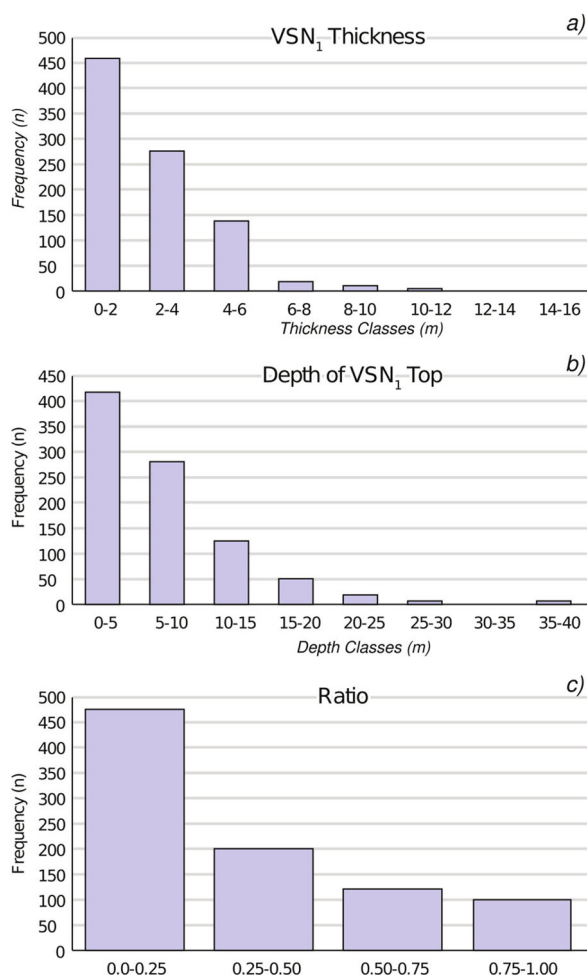
Figure 9. Frequency distributions of values of relevant geological information sampled from the subsoil geological model in sinkhole locations: VSN_1 thickness (a), depth from the surface of the top of VSN_1 layer (b) and ratio of VSN_1 thickness to the depth of its bottom (c).

the surface): the larger the depth, the smaller the sinkhole frequency (Figure 9b). In general terms, this last evidence could seem partly not consistent with the expected effect of increasing geostatic loads acting on cavity roofs, but at the same time, a larger depth implies the possibility to accommodate the formation of arch effect as well as a longer path for the 'migration' of the tunnel roof up to the ground surface.

- The ratio of VSN_1 thickness to the depth of its bottom, which expresses the proportion of cover made up of materials with fair geomechanical properties, plotted versus the sinkhole occurrence clearly shows that the latter occur more frequently where this proportion is low (Figure 9c), thus indicating an overall poor geomechanical quality of deposits covering (and then, protecting) the cavity network.

Based on this evidence, the geo-thematic variables have been considered together with the density of known cavities (i.e. the most reliable proxy of underground cavity presence

Tab 1. Summary statistics of the values assumed by the parameters considered in the multivariate analysis.

Variable	Max	Min	Mean	Standard dev
Cavity density	269.1	0	11.8	26.2
VSN_1 thickness	18.9	0	1.9	2.7
VSN_1 top depth	37.6	0	4.3	6.7
Ratio (VSN_1 thickness/ VSN_1 bottom depth)	0.99	0	0.33	0.38

and, thus, the most relevant information for the process under study) in performing the multivariate analysis. Table 1 summarizes the values variability of each factor considered in the analysis. As regards the variable importance, expressed in terms of coefficients of the Logit function, cavity density and the ratio of VSN_1 thickness to the depth of its bottom have the major weight in favoring the process of sinkhole formation. Accuracy of the predictive model was assessed for the training subset by random space validations availing of Receiver Operating Characteristics (ROC) curves. Area Under Curve (AUC) equal to 0.91 was computed in the training stage. The predictive capability of the logistic model has been also tested in an area not considered in the training (i.e. multi-spatial validation). This test results in AUC equal to 0.9, which proves the good performance of the model, as most of the actual sinkholes fall into high SHS zones as well as stable areas were adequately predicted (Figure 10).

By applying the validated Logit function to the study area, it was possible to provide a map that represents a zonation of the territory in terms of Sinkhole Susceptibility (SHS) resulting from the spatial correlation of every factor in each single cell ($5 \times 5\,m$) in which the area is partitioned. Since the final results are expressed for each raster cell in terms of probability, thus ranging from 0 to 1, to belong to class '1' (i.e. sinkhole occurrence), the obtained map was classified into 5 equal interval classes (i.e. class $1 = 0$–0.19, class $2 = 0.2$–0.39, class $3 = 0.4$–0.59, class $4 = 0.6$–0.79, class $5 = 0.8$–1): the higher the class number, the higher the proneness to sinkhole occurrence.

Furthermore, areas resting on alluvial deposits or hosting main infrastructures (such as railway lines and main roads) have been superimposed on the final SHS map (Figure 10), as related ground deformations cannot be uniquely ascribed to anthropogenic sinkholes predictors but also to 'conventional' subsidence and/or settlement effects.

4.2. A-Dinsar analyses

4.2.1. PS filtering
The Sentinel-1 datasets related to PSs lying on the ground have been filtered according to the procedure previously described. In the following, the main outcomes of a supervised application of developed algorithms are listed.

1. Phase coherence. Following accurate evaluations and empirical tests, only PSs with phase coherence > 0.7 have been selected, thus reducing the initial dataset by about 45% in both orbits.
2. Retrieval of temporary scatterers based on the identification of T_{on} and T_{off}, as described in the previous section.
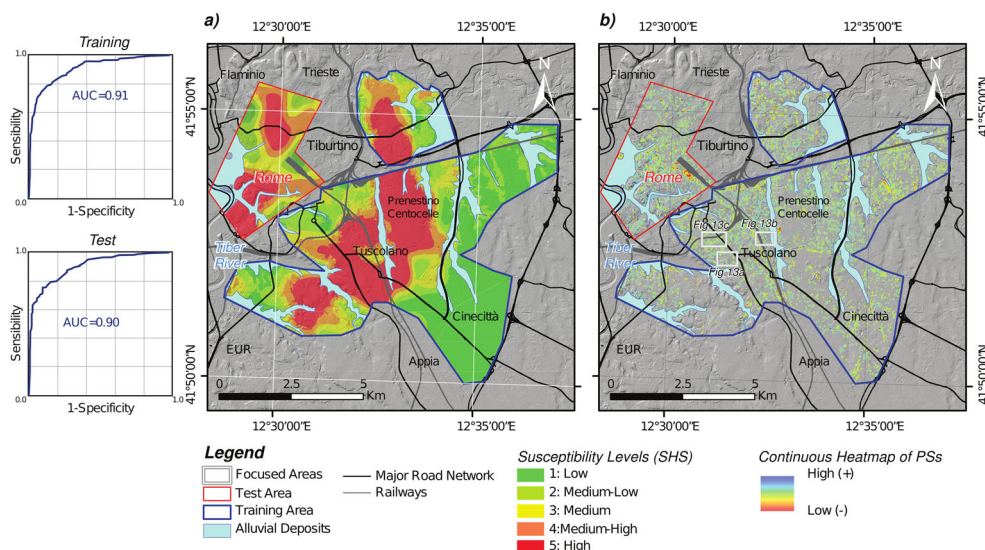
Figure 10. a) Sinkhole Susceptibility map; ROC curves and related AUC values obtained in the training and test areas are reported on the left. b) Heatmap of subsiding PSs selected after A-DInSAR filtering of the CSK dataset.

3. Standard deviation (σ) of time-histories of displacements: following accurate assessments and empirical tests, PSs with standard deviation values $2\sigma = \pm 6.25$mm have been excluded to filter only the targets with the most accurate time series of displacements; a further reduction of about 10% of the original dataset has been obtained for both orbits.

4. Velocity and sense of movement. From the in-depth analysis of the original dataset, it was possible to provide a rough assessment of the accuracy values in estimating the average annual PS velocity (approximately $\pm$ 2mm/year). To select only PSs that recorded reasonably reliable displacements during the monitoring period and to exclude, therefore, all those that did not detect appreciable displacements, the threshold of 2.5 mm/year (thus exceeding the estimated accuracy threshold) has been selected. Specifically, only PSs with negative values (therefore moving away from the sensor) with an average velocity < -2.5 mm/year, have been selected. This last selection significantly reduced the number of PSs considered reliable, which are 2.3% and 1.9% of the original datasets for the ascending and descending orbits, respectively.

The same filters have been applied to CSK datasets and the related maps of PS cumulated displacement were produced (Figure 11).

4.2.2. Temporal and spatial prediction of sinkhole occurrence

To test the capability of SAR products in detecting the incipient formation of sinkholes, Sentinel-1 and CSK processed datasets have been used to back-analyze some selected cases of sinkholes that occurred on a known date. Specifically, we back-analyzed 3 sinkholes that occurred in the time interval 11 January 2017–18 December
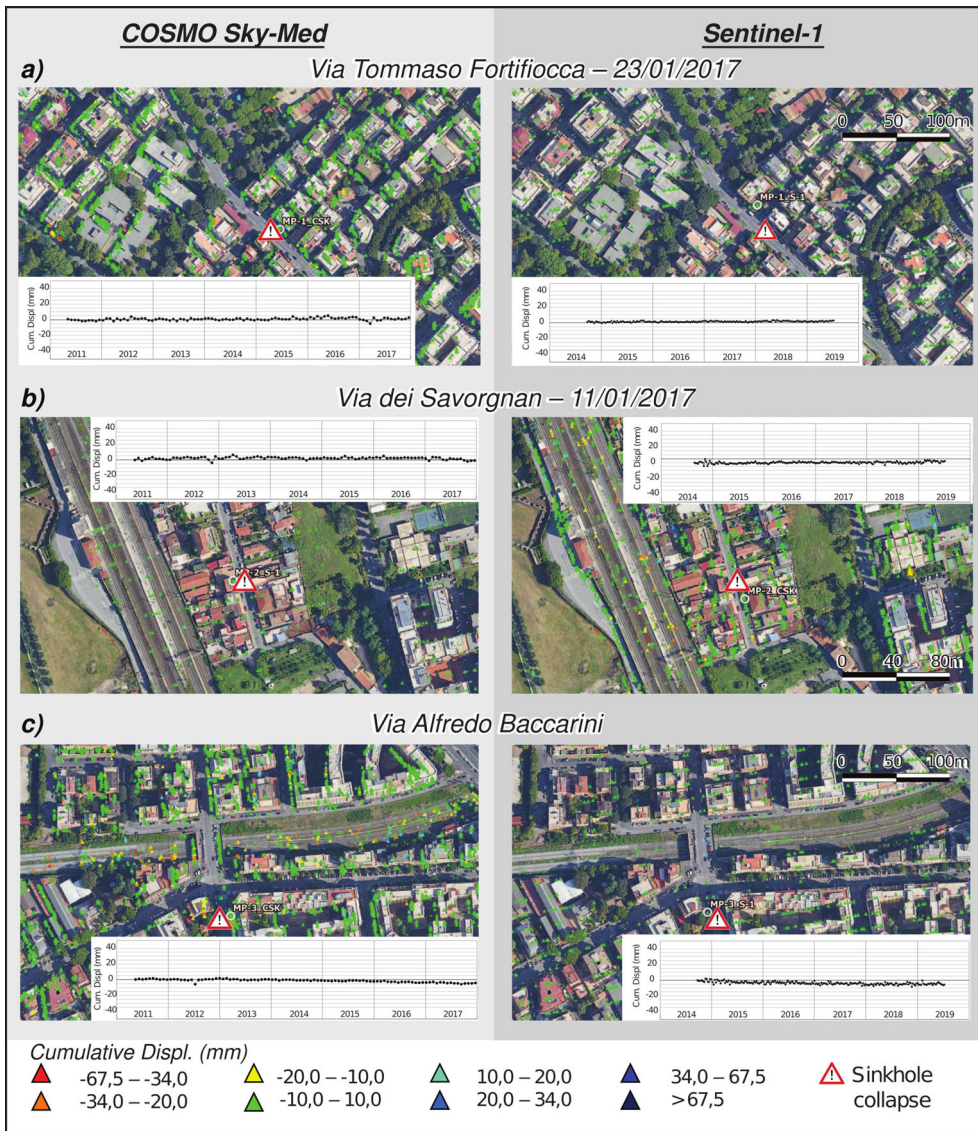
Figure 11. Maps of PS displacements derived from A-DinSAR processing of COSMO Sky-Med (left) and Sentinel-1 (right) in three different areas of interest, where sinkholes occurred. Time-series of displacement are also reported.

2017. The results show that a deformation process preceding the collapse is not clearly detectable in any of the 3 cases, nor through CSK (Figure 11). The analysis has been repeated also with datasets filtered with less 'severe' thresholds, to verify possible effects of PS removal; the overall results did not change. In terms of detection of critical areas, regardless of the maturity stage of the process, the velocity maps allowed us to preliminary observe spatial clusters of subsiding PSs on a quite constant background of stable points (Figure 12); this geometrical feature already suggests a very localized process, a sort of punctual anomaly (if referred to the large-scale) consistent with the spatial pattern of an incipient sinkhole.
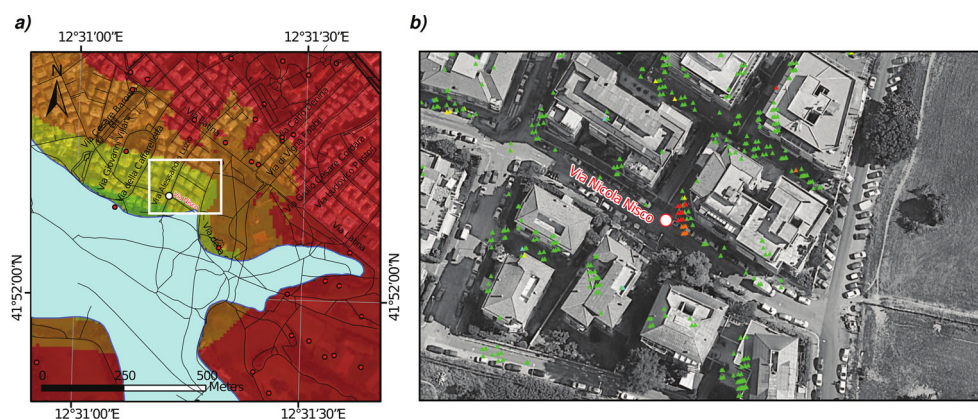
Figure 12. Spatial prediction of sinkhole occurrence in areas of medium susceptibility highlighted by clustering of subsiding PSs in Via Nisco, where a ground lowering related to incipient sinkhole took place in April 2017.

Furthermore, a preliminary overlay with the SHS map showed a frequent occurrence of these clusters in medium to high susceptibility zones (Figure 12). Based on this evidence, we consider that useful information can be provided by a method for the automatic recognition of such clusters by interpolating the values of 'anomalous' PS concentrations over a constrained neighborhood, thus resulting in zonation of the territory based on heatmaps. This procedure relies on KDE functions recalled in the Section 3 and has been refined and implemented by applying the following functions and parameters:

- A bi-weight Kernel function with a bandwidth of 20 m has been selected, which quantifies the influence of actual measures on values to be estimated in locations without direct measures in the form given below:

$$P(x) = \frac{15}{16}(1 - d^2)^2 \tag{1}$$

W re 'x' is the location of the point (centroid of a raster cell) where a density value has to be assigned and 'd' is the Euclidean distance from the PS in the given neighborhood divided by the Kernel bandwidth.

- The density also takes into account the average velocity of PSs, so (1) turns into:

$$P(x) = Vel_{PS}\ \frac{15}{16}(1 - d^2)^2 \tag{2}$$

- If a point falls in the radius of influence of 'n' PSs, (2) turns into

$$P(x) = \sum_{i=1}^{n}\left[Vel_{PS}\ \frac{15}{16}(1 - d^2)^2\right] \tag{3}$$

The obtained heatmaps of filtered subsiding PSs (fSP), exemplified in Figure 10, have been classified into two classes (High and Medium concentrations of

'anomalous' PSs) with a break value of 18 (Figure 13). Areas with values less than 3 are considered as not significant and defined as a Low concentration class.

4.2.3. Data integration

On a monthly basis, or in any case equal to the supply frequency of the satellite SAR dataset by ACEA, the PS filtering actions must be repeated until the production of the fSP heatmaps (Figure 13).

The latter, referring to the ascending and descending satellite orbits, can be integrated and overlaid to produce a combined fSP (C_fSP) heatmap that considers the presence of areas of attention in only one of the two orbits or both. Considering that each heatmap is produced for each orbit and the results are classified in two classes (Medium and High concentration), a summary map, obtained through a series of analytical overlay procedures (intersect – erase – merge), has been obtained and reclassified based on growing criticality potential as follows:

- Class 1: areas identified in a single orbit and with a Medium value of PS concentration
- Class 2: areas identified in both orbits and with a Medium value of PS concentration
- Class 3: areas identified in both orbits (one with a Medium value and the other with a High value of PS concentration)
- Class 4: areas identified in both orbits and with a High value of PS concentration

The information obtained still does not allow to attribute any cause-effect principle between observed deformation and governing process. Clues to this can be drawn by a geological interpretation of the potential processes detected and represented in the summary heatmap. Hence, the latter has been intersected with the classified SHS map: the possible combination of 5 SHS classes with the 4 concentration classes of the C_fSP heatmap described above, is summarized in a map expressing the integrated levels of subsiding PSs concentration and sinkhole susceptibility (C_fSP/SHS), that highlights the 'hotspots' to focus on as potential precursor of underground cavity collapse (Figure 14).

On this base, the critical areas identified by interferometry have been further reclassified and hierarchized, in four classes in their turn subdivided into five subclasses according to the actual likelihood that they are affected by incipient processes of sinkhole collapse due to the evolution of pre-existing underground cavities. This represents the final product to support subsequent decisions on the management of such potential criticalities, by means of detailed investigations, monitoring and preventive remediation interventions.

5. Discussion

As regards sinkhole susceptibility analysis (Section 4.1), which in this work represents the interpretative filter of the SAR data, the most relevant results can be summarized as follows: the main predisposing factor is the density of existing anthropogenic cavities, as expected since it represents a proxy of the actual presence of cavities, which is a necessary condition for the process under study to occur. But at the same time
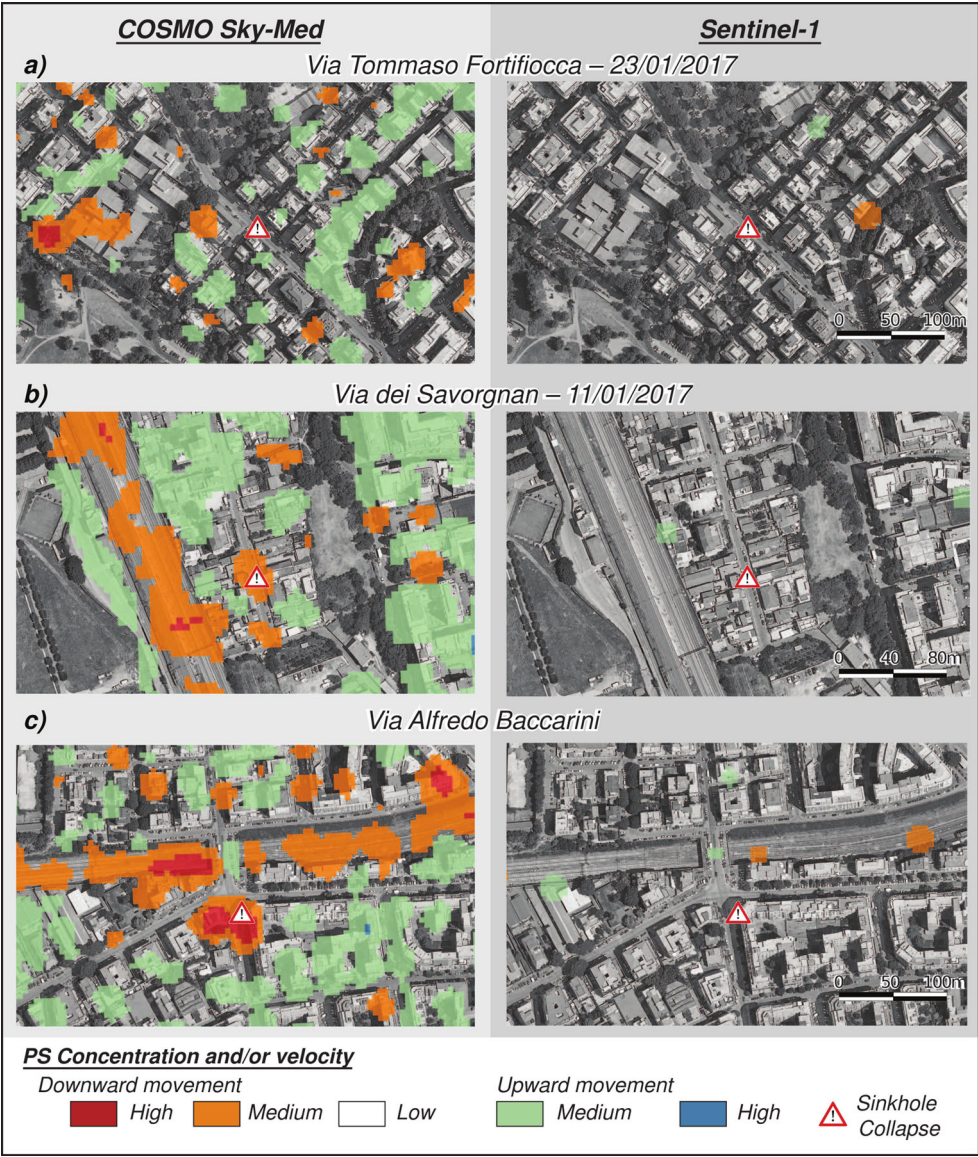
Figure 13. Classified fSP heatmaps derived from A-DinSAR processing of COSMO Sky-Med (left) and Sentinel-1 (right) in three different areas of interest, where sinkholes occurred.

geo-thematic information, in turn consistent with known conceptual models of cavity development up to the formation of ground collapses, are useful to better grade and refine the predisposition to failure of the adopted mapping units. The availability (and reliability) of a geological model representing the 'significant' subsoil volume (i.e. at least up to the depth where the process starts) plays a relevant role for an effective hazard zoning. Beyond the statistical indicators of accuracy (e.g. ROC curves), the effective predictive capability of the susceptibility analysis can be independently assessed by comparing the location of sinkholes occurred after having performed the analysis and the predicted susceptibility value (or class), which represents
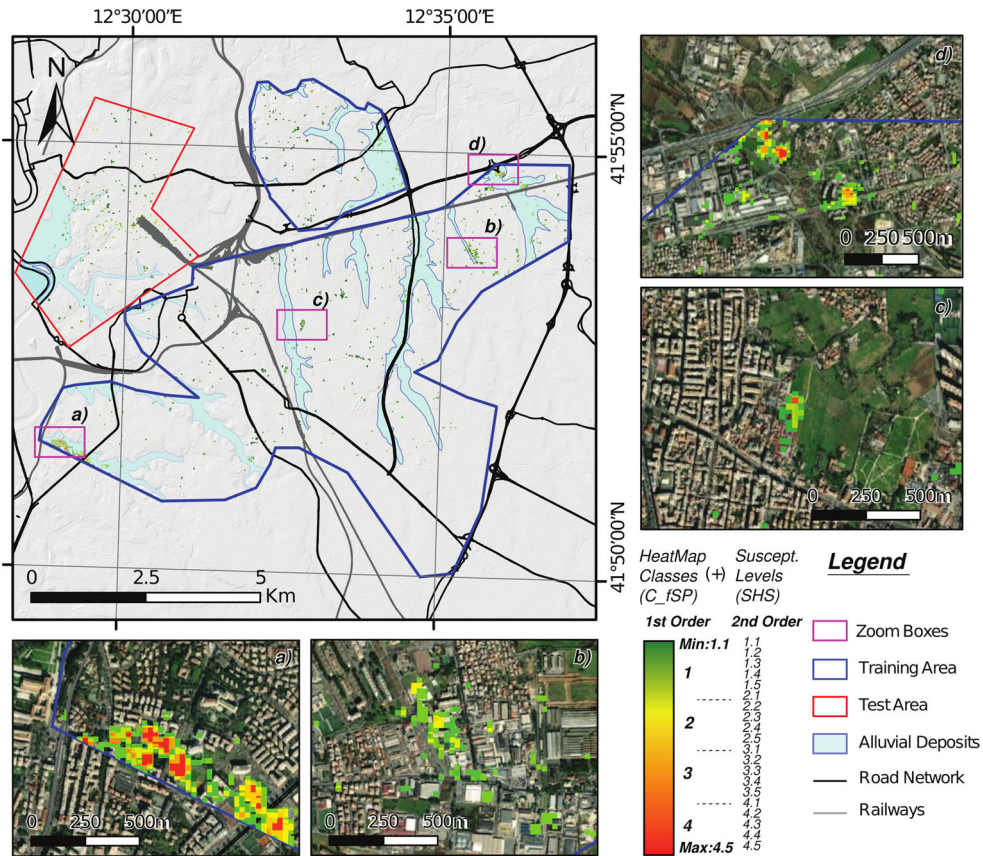
Figure 14. Map showing 'hotspots' in terms of integrated levels of subsiding PSs concentration and sinkhole susceptibility (C_fSP/SHS map).

a temporal validation *sensu* Chung and Fabbri (2003): the recent case of Via Zenodossio, where a sinkhole occurred in correspondence of a pixel in the SHS map belonging to the highest susceptibility class (and with a value of predicted susceptibility of 94.5%) gives further strength to the analysis results (Figure 15a).

The velocity maps (Section 4.2) allowed us to observe spatial clusters of subsiding PSs. In this regard it is worth highlighting that a sinkhole recently (and after the analysis presented in this paper) occurred roughly in correspondence of the cluster of subsiding PSs of Figure 12 in via Nicola Nisco (Figure 15b), thus revealing the potential to exploit the monitoring dataset at least as a tool for the territory zoning in terms of spatial hazard. In fact, with appropriate post-processing operations of the data with both filter algorithms and geospatial processing of the data thus filtered, it is possible to identify areas with potential criticality in progress ('hotspots') (Figure 14). The integration of the two products (SHS and C_fSP) represents the core of the interpretation of the displacement data: understanding if the actual presence of ground deformations in progress – hotspots – is likely correlated to incipient sinking processes, based on the independent sinkhole spatial susceptibility analysis. This integration can be regarded as data assimilation as defined in the work of Abspoel et al. (2018). Furthermore, the achieved results allowed us to analyze the main differences
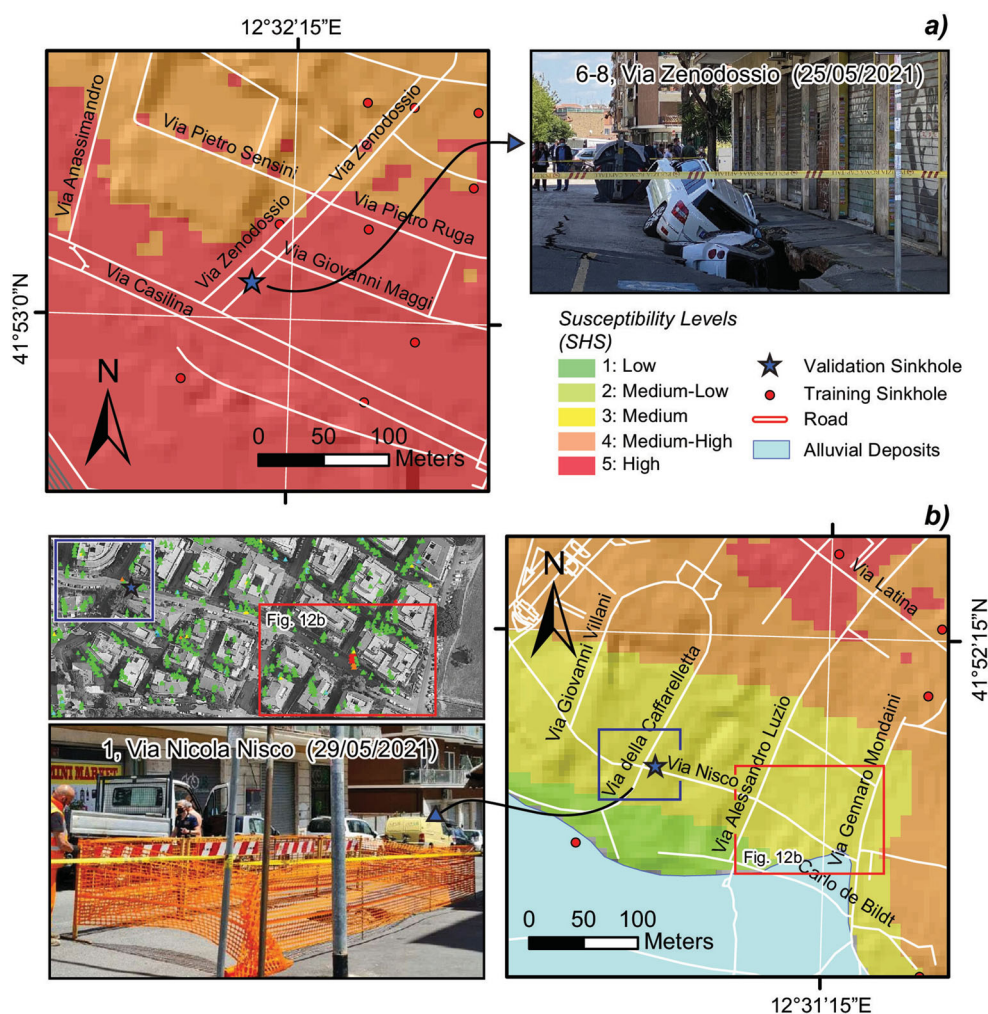
Figure 15. Location of the sinkholes occurred in Via Zenodossio (a) and Via Nisco (b) in May 2021 (and, thus, not included in the training dataset of the susceptibility function) compared with the results of the analyses carried out in this study.

between the SAR datasets (respectively from Sentinel-1 and COSMO-SkyMed satellites). As discussed, by way of example, also in Comut et al. (2016), even though the temporal and spatial baselines of COSMO-SkyMed are generally greater than Sentinel-1, the achieved results from COSMO-SkyMed and Sentinel-1 data processing in terms of PSs velocity estimation, over the same area and approximately the same period, are comparable, thus validating the reliability of an integrated approach. Other examples of integrated approaches based on COSMO-SkyMed and Sentinel-1 data in different part of the world are also discussed in Costantini et al. (2017) (monitoring of surface deformations in wide areas) and Jung et al. (2019) (long-term deflection monitoring of bridges).

The higher and isotropic spatial resolution of COSMO-SkyMed SAR images ($\sim$3 $\times$ 3 m) significantly impacts the density of information, providing a much greater number of PSs with respect to the medium resolution Sentinel-1 dataset ($\sim$5 $\times$ 20 m). This allows to perform a more detailed screening and to detect local spatial anomalies

affecting small areas (typical of sinkholes in urban areas). Moreover, the COSMO-SkyMed sensor (X-Band) is characterized by a higher sensitivity in detecting small movements and estimating the heights of PS, suitable for a more effective selection procedure. Nevertheless, the significantly lower revisit time and revisit regularity with respect to the Sentinel-1 satellite, may have a negative impact on the early detection of collapse precursors.

One of the aspects that deserve attention is related to the attempt to test the capability of SAR monitoring to forecast the time to failure and, thus, to represent a more efficient tool to optimize risk reduction strategies, especially in terms of resilience enhancement. In the case we examined, it was not possible through the back-analysis to define a temporal trend of deformations typical of the pre-failure phase, thus making it impossible to define critical thresholds for the purpose of early warning by means of a mere analysis of interferometric data. The possible causes are of a different nature: from the more strictly technical ones to those more related to the peculiarity of the process. As regards technical issues, our interpretation is that the absence of pre-collapse information is mainly linked to the lack of PS exactly in the future sinkhole areas (lower number of PS on the roads, the typical location for sinkhole formation) and their size (only a few square meters wide) and not to the certain absence of pre-failure deformations. With reference to the specific process, the shape of the signal related to the surface deformation temporal trend could be quite complicate as it records an intermittent process made of alternation of steady phases (weathering and weakening of the rooftops giving no or negligible ground deformations) and sudden accelerations (failure of the rooftops) as well as can be affected by the presence and variability of anthropic dynamic loads. The successful cases of SAR satellite techniques in this sense do not lack, as well documented and analyzed in the work of Theron and Engelbrecht (2018) which offers many hints also on the limits of the technique in and of itself; but it should be noted that they are often relative to cases in which both the type of sinkhole (mainly by dissolution) and their size (often tens of meters), as well as the environmental context, differ significantly from that considered in this work.

The analyzed cases, in fact, were formed on the road surface where it is extremely difficult to find valid and reliable reflectors for the purposes of interferometric analysis.

6. Conclusions

The experience gained in the application to the Rome case study allows us to draw some broader considerations.

The first consideration concerns the data assimilation: once again and following the previous experience gained in the Roman coastal area by the Authors (Bozzano et al. 2018) we demonstrate that the contribution of satellite SAR monitoring for the management of the risk linked to specific geological processes, can be maximized only if superimposed with other independent and relevant information on the geological processes themselves.

This is even more evident in the urban context in which advantages (presence of several reflectors) and disadvantages (background noise and displacements conditioned by

the deformation response of structures) of this monitoring technique applied to geo-logical risks are magnified. The issue becomes even more critical with reference to the specific process of anthropogenic sinkholes of reduced areal extension. At least in terms of spatial detection capacity, we demonstrate that the most effective filter to screen the monitoring data and focus the attention only on those most likely related to the process of interest is represented by the overlap with data and information derived from an inde-pendent evaluation and related zoning of the predisposition to that type of instability. In addition to the aforementioned phenomenological filter, the interferometric filter is not of secondary importance, as in the case of the sequence of algorithms that already in a preliminary phase allows to eliminate the 'background noise' and to select the most robust data for the definition of the process of interest.

As regards the specificity of the analyzed geological hazard – formation of sinkholes in the eastern part of Rome urban area – to date it was not possible to accredit SAR interfer-ometry for forecasting purposes in terms of capability to predict the time of failure.

However, following the results of the here reported analyses and aiming at the reduction of the pipeline system vulnerability by means of non-structural measures, an operational procedure has been set-up and is now in the testing phase to assess and periodically update the sinkhole spatial hazard and activate attention and control protocols. The procedure involves the following steps:

1. periodic acquisition of updated satellite SAR data, processing and identification of hotspots
2. priority classification of hotspots by overlapping with susceptibility information.
3. activation of procedures to verify the actual state of the pipelines through site inspections.
4. check with standard geophysical techniques (micro-gravimetry, geoelectrical investigations, etc.) of the actual presence of cavities and, according to the results, design and implementation of site-specific remediations interventions or high-resolution monitoring.

Acknowlegment

Disclosure statement

No potential conflict of interest was reported by the authors.

ORCID

Carlo Esposito http://orcid.org/0000-0001-5429-2959
Francesca Bozzano http://orcid.org/0000-0002-0297-842X
Gian Marco Marmoni http://orcid.org/0000-0002-0443-4389
Paolo Mazzanti http://orcid.org/0000-0003-0042-3444
Saverio Romeo http://orcid.org/0000-0002-9323-6308

Data availability statement

The data that support the findings of this study are available from the corresponding author, C.E., upon reasonable request.

References

Absp l L, Courage W, Dabekaussen W, de Bruijn R, Kruse H, Wiersma AP, Hijma MP, van den Heuvel F, van den Broeck W. 2018. Risk-based asset management: automated structural reliability assessment of geographically distributed pipeline networks for gas and water in the Netherlands. Struct Infrastruct Eng. 14(7):928–940.

Bianchi Fasani G, Bozzano F, Cercato M. 2011. The underground cavity network of south-eastern Rome (Italy): an evolutionary geological model oriented to hazard assessment. Bull Eng Geol Environ. 70(4):533–542.

Bozzano F, Ciampi P, Del Monte M, Innocca F, Luberti GM, Mazzanti P, Rivellino S, Rompato M, Scancella S, Scarascia Mugnozza G. 2020. Satellite A-DInSAR monitoring of the Vittoriano monument (Rome, Italy): implications for heritage preservation. Ital J Eng Geol Environ. 2:5–17.

Bozzano F, Esposito C, Mazzanti P, Patti M, Scancella S. 2018. Imaging multi-age construction settlement behaviour by advanced SAR interferometry. Remote Sens. 10(7):1137.

Cascini L. 2008. Applicability of landslide susceptibility and hazard zoning at different scales. Eng Geol. 102(3–4):164–177.

Chang L, Hanssen RF. 2014. Detection of cavity migration and sinkhole risk using radar interferometric time series. Remote Sens Environ. 147:56–64.

Chung CJF, Fabbri AG. 2003. Validation of spatial prediction models for landslide hazard mapping. Nat Hazards. 30(3):451–472.

Ciotoli G, Corazza A, Finoia MG, Nisio S, Serafini R, Succhiarelli C. 2013. Sinkholes antropogenici nel territorio di Roma Capitale. Mem Descr Carta Geol d'It. 93:143–181.

Ciotoli G, Nisio S, Serafini R. 2015. Analisi della suscettibilità ai sinkholes antropogenici nel centro urbano di Roma: analisi previsionale. Mem Descr Carta Geol d'It. 99:167–188.

Comut FC, Ustun A, Lazecky M, Perissin D. 2016. Capability of detecting rapid subsidence with Cosmo SkyMed and Sentinel-1 dataset over Konya city. Proceedings of the ESA Living Planet Symposium, ESA SP740, Prague, Czech Republic, p. 9–13.

Costantini M, Ferretti A, Minati F, Falco S, Trillo F, Colombo D, Novali F, Malvarosa F, Mammone C, Vecchioli F, et al. 2017. Analysis of surface deformations over the whole Italian territory by interferometric processing of ERS, Envisat and COSMO-SkyMed radar data. Remote Sens Environ. 202:250–275.

Ferretti A, Prati C, Rocca F. 2000. Nonlinear subsidence rate estimation using permanent scatterers in differential SAR interferometry. IEEE Trans Geosci Remote Sens. 38(5):2202–2212.

Ferretti A, Prati C, Rocca F. 2001. Permanent scatterers in SAR interferometry. IEEE Trans Geosci Remote Sens. 39(1):8–20.

Funiciello R, Giordano G. 2008. The geological map of Rome: lithostratigraphy and stratigraphic organization. La Geologia di Roma. Dal Centro Storico Alla Periferia II. Mem Desc Carta Geologica D'Italia. 80:39–85.

Galve JP, Gutiérrez F, Lucha P, Guerrero J, Bonachea J, Remondo J, Cendrero A. 2009. Probabilistic sinkhole modelling for hazard assessment. Earth Surf Process Landforms. 34(3):437–452.

Galve JP, Remondo J, Gutiérrez F. 2011. Improving sinkhole hazard models incorporating magnitude–frequency relationships and nearest neighbor analysis. Geomorphology. 134(1–2):157–170.

Gencer EA. 2017. How to make cities more resilient: a handbook for local government leaders. United Nations Office for Disaster Risk Reduction. erry Velasquez and Abhilash Panda (UNISDR) 122 p. Geneva.

Gernhardt S, Adam N, Eineder M, Bamler R. 2010. Potential of very high resolution SAR for persistent scatterer interferometry in urban areas. Ann GIS. 16(2):103–111.

Godschalk DR. 2003. Urban hazard mitigation: creating resilient cities. Nat Hazards Rev. 4(3): 136–143.

Hanssen RF. 2005. Satellite radar interferometry for deformation monitoring: a priori assessment of feasibility and accuracy. Int J Appl Earth Obs Geoinf. 6(3–4):253–260.

Intrieri E, Gigli G, Nocentini M, Lombardi L, Mugnai F, Fidolini F, Casagli N. 2015. Sinkhole monitoring and early warning: an experimental and successful GB-InSAR application. Geomorphology. 241:304–314.

Jung J, Kim DJ, Palanisamy Vadivel SK, Yun SH. 2019. Long-term deflection monitoring for bridges using X and C-band time-series SAR interferometry. Remote Sens. 11(11):1258.

Kampes BM. 2006. Radar interferometry: persistent scatterer technique. Berlin/Heidelberg: Springer.

Kersten T, Kobe M, Gabriel G, Timmen L, Schön S, Vogel D. 2017. Geodetic monitoring of subrosion-induced subsidence processes in urban areas: concept and status report. J Appl Geodesy. 11(1):21–29.

Lee EJ, Shin SY, Ko BC, Chang C. 2016. Early sinkhole detection using a drone-based thermal camera and image processing. Infrared Phys Technol. 78:223–232.

Malinowska AA, Witkowski WT, Hejmanowski R, Chang L, van Leijen FJ, Hanssen RF. 2019. Sinkhole occurrence monitoring over shallow abandoned coal mines with satellite-based persistent scatterer interferometry. Eng Geol. 262:105336.

Marra F, Florindo F. 2014. The subsurface geology of Rome: sedimentary processes, sea-level changes and astronomical forcing. Earth Sci. 136:1–20.

Marra F, Rosa C. 1995. Stratigrafia e assetto geologico dell'area romana. Memorie Descrittive Della Carta Geologica D'Italia. 50:49–118.

Nisio S, Allevi A, Ciotoli G, Ferri G, Fiore R, Pascucci R, Stranieri I, Succhiarelli C. 2017. Carta Delle Cavità Sotterranee Di Roma. ISPRA online publication. https://www.isprambiente.gov.it/it/attivita/suolo-e-territorio/cartografia/carta-delle-cavita-sotterranee-di-roma

Nof RN, Abelson M, Raz E, Magen Y, Atzori S, Salvi S, Baer G. 2019. SAR interferometry for sinkhole early warning and susceptibility assessment along the Dead Sea, Israel. Remote Sens. 11(1):89.

Orhan O, Oliver-Cabrera T, Wdowinski S, Yalvac S, Yakar M. 2021. Land subsidence and its relations with sinkhole activity in Karapınar Region, Turkey: a multi-sensor InSAR time series study. Sensors. 21:774.

Orhan O, Yakar M, Ekercin S. 2020. An application on sinkhole susceptibility mapping by integrating remote sensing and geographic information systems. Arab J Geosci. 13(17):886.

Parise M, Ravbar N, Živanović V, Mikszewski A, Kresic N, Mádl-Szőnyi J, Kukurić N. 2015. Hazards in karst and managing water resources quality. In: Stevanovic Z, editor. Karst aquifers – characterization and engineering. Cham: Springer; p. 601–687.

Pradhan B, Abokharima MH, Jebur MN, Tehrany MS. 2014. Land subsidence susceptibility mapping at Kinta Valley (Malaysia) using the evidential belief function model in GIS. Nat Hazards. 73(2):1019–1042.

Theron A, Engelbrecht J. 2018. The role of earth observation, with a focus on SAR Interferometry, for sinkhole hazard assessment. Remote Sens. 10(10):1506.

Vaccari A, Batabyal T, Tabassum N, Hoppe EJ, Bruckno BS, Acton ST. 2018. Integrating remote sensing data in decision support systems for transportation asset management. Transp Res Rec. 2672(45):23–35.

Ventriglia U. 2001. Geologia del territorio del Comune di Roma. Amministrazione Provinciale di Roma, Servizio Geologico, Difesa del Suolo.

Waltham T. 2008. Sinkhole hazard case histories in karst terrains. Q J Eng Geol Hydrogeol. 41(3):291–300.

Wang Z, Balz T, Zhang L, Perissin D, Liao M. 2018. Using TSX/TDX pursuit monostatic SAR stacks for PS-InSAR analysis in urban areas. Remote Sens. 11(1):26.